Journal of Materials Chemistry A

PAPER

View Article Online
View Journal | View Issue

Cite this: J. Mater. Chem. A, 2016, 4, 2332

Synthesis, characterization and *ab initio* investigation of a panchromatic ullazine–porphyrin photosensitizer for dye-sensitized solar cells†

Simon Mathew,‡*[a] Negar Ashari Astani,[b] Basile F. E. Curchod,§[b] Jared H. Delcamp,¶[a] Magdalena Marszalek,††[a] Julien Frey,‖[a] Ursula Rothlisberger,[b] Mohammad Khaja Nazeeruddin[a] and Michael Grätzel[a]

Received 29th October 2015
Accepted 19th January 2016

DOI: 10.1039/c5ta08728g

www.rsc.org/MaterialsA

An ullazine unit was employed as a donor moiety in a donor–π–acceptor (D–π–A) motif, employing the porphyrin macrocycle as a π-system. Synthesis of this ullazine–porphyrin dyad containing sensitizer (**SM63**) was achieved and an investigation of the electrochemical and spectroscopic properties of this dye was performed. Introduction of the ullazine donor promoted significant enhancements in long and visible wavelength absorption, leading to panchromatic light harvesting. **SM63** demonstrated a maximum absorption approaching 750 nm, a significant improvement compared to the model compound **LD14-C8**, which features a simpler donor component (4-(*N*,*N*-dimethylamino)phenyl) and an absorption onset at ~700 nm. The dye **SM63** was subjected to a rigorous *ab initio* investigation to gain further insight into its unique absorption and emission properties. Application of the molecular ullazine–porphyrin dyad **SM63** into dye-sensitized solar cells afforded a device with significantly improved light harvesting abilities in both the visible region of the spectrum as well as NIR light (~800 nm), demonstrating the value of ullazine unit in developing panchromatic dyes for light harvesting applications.

Introduction

The porphyrin core remains a prominent choice as a π-bridge in the design of D–π–A dyes for application in dye-sensitized solar cells (DSCs), with the porphyrin based dye **YD2-o-C8** achieving power conversion efficiencies (PCEs) of 11.9%.[1] This remarkable result was improved to 12.3% by cosensitization with the dye **Y123**, possessing complementary absorbance to the green porphyrin sensitizer, thereby increasing the short-circuit current density (J_{SC}) of the DSC through enhancing the light harvesting efficiency of the device. In order to improve the overall PCE of the DSC, strategies must be explored to engineer dyes with panchromatic light harvesting abilities. Significant efforts have been undertaken in investigating the use of new, novel electron accepting units that can impart significant perturbations of the porphyrinic electronic structure in order to improve visible light absorption.[2,3] In particular, this brand of molecular engineering results in dyes like **SM315** that exhibit improved visible and infrared light harvesting resulting in a PCE of 13%, when used in conjunction with cobalt-based redox electrolytes.[4,5]

In a complementary manner, there has been much work exploring the utility of alternative π-systems as donor groups for porphyrin dyes connected to the central porphyrin core *via* an acetylene bridge.[6–13] All of these dyes exhibited moderate to high performance with iodide/triiodide redox electrolytes. However, a common feature of all such dyes with π-extended donors possess very similar absorbance features, exhibiting a deficit in green light harvesting ability (~550 nm), due to the poor absorption between characteristic porphyrinic B- (Soret) and Q-bands.

The ullazine chromophore is a 16 π-electron heterocycle, isoelectric to pyrene exhibiting simultaneous electron donating and accepting properties.[14,15] Recently, the utility of this heteroarene was demonstrated by exploiting it as a π-bridge in DSCs.[16,17] Of significant value from these investigations was the development of facile synthetic route to meaningful quantities

[a]*Laboratory of Photonics and Interfaces (LPI), École Polytechnique Fédérale de Lausanne (EPFL), CH-1015, Lausanne, Switzerland. E-mail: s.mathew@uva.nl*

[b]*Laboratory of Computational Chemistry and Biochemistry (LCBC), École Polytechnique Fédérale de Lausanne (EPFL), CH-1015 Lausanne, Switzerland*

† Electronic supplementary information (ESI) available: Synthetic procedures, computational details, absorption/fluorescence spectra, photovoltaic data for optimization of DSCs, HRMS and NMR data. See DOI: 10.1039/c5ta08728g

‡ Current address: van 't Hoff Institute for Molecular Sciences, Universiteit van Amsterdam, Science Park 904, 1098 XH Amsterdam, The Netherlands. Email: s.mathew@uva.nl

§ Current address: Department of Chemistry, Stanford University, Stanford, CA 94305-4401, USA.

¶ Current address: Department of Chemistry, University of Mississippi University, MS 38677, USA.

†† Current address: Department of Physics and Astronomy, Faculty of Sciences, Vrije Universiteit Amsterdam, De Boelelaan 1081, 1081 HV, Amsterdam, The Netherlands.

‖ Current address: Novaled GmbH, Tatzberg 49, 01307 Dresden, Germany.

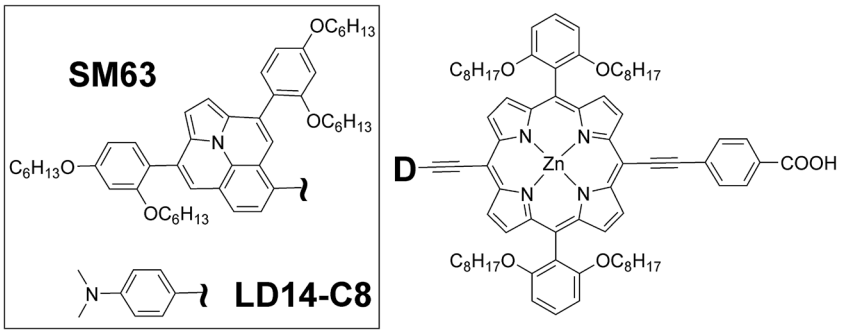

Fig. 1 Structure of the SM63 and LD14-C8 sensitizers.

of the ullazine core. From this ullazine synthon, the installation of functional groups can facilitate the application of this unique heterocycle in molecular constructs of increasing structural and electronic complexity.

In this work we introduce the ullazine aromatic system as a potential starting point for donors that impart panchromatic absorption to the porphyrin D–π–A framework. We present the first ullazine–porphyrin dyad **SM63** (Fig. 1), which is additionally functionalized with an ethynylbenzoic acid as an anchoring group, allowing the corresponding dye to bind to the TiO_2 photoanode within the DSC.

Results and discussion

Synthesis

The ullazine–porphyrin dyad **SM63** is outlined in Scheme 1. An alkyne-functionalized ullazine **2** was coupled to the *meso*-dibrominated zinc porphyrin core **3**. The alkynyl-functionalized ullazine **2** was synthesized from the previously reported formyl-ullazine synthon **1** (ref. 18) *via* a Corey–Fuchs reaction. Specifically, an initial Wittig reaction of **1** with dibromomethyl-triphenylphosphonium bromide followed by elimination by *t*-BuOK yielded the alkyne-functionalized ullazine synthon **2** in a 71% yield. Subsequent Sonogashira coupling of this ullazine unit with the previously reported porphyrin component, 5,15-dibromo-10,20-(2,6-dioctyloxyphenyl)porphyrinatozinc(II) **3** (ref. 7) followed by coupling with the 4-ethynylbenzoic acid anchor afforded the complete dye **SM63** in Fig. 1. The dye **LD14-C8** (ref. 7) was employed as a reference compound to enable comparison to typical porphyrin dyes possessing an acetylene linked 4-dimethylaminophenyl donor and ethynylbenzoic acid acceptor. **SM63** was characterized by ^{1}H and ^{13}C NMR spectroscopy and HRMS (ESI†).

UV-Vis spectrophotometric properties

The UV-Vis absorbance spectrum of **SM63** was performed in THF solvent (Fig. 2) and compared to **LD14-C8**, with the relevant data summarized in Table 1. Substitution of the ullazine moiety into the porphyrin core caused a severe deformation of the Soret band in the absorption spectrum of **SM63**. The introduction of the ullazine donor into the dye structure triggered more excitations leading to a broadening of the Soret band. The experimental spectrum of **SM63** affords two discernable Soret absorbances, with the dominant one at 450 nm with a shoulder

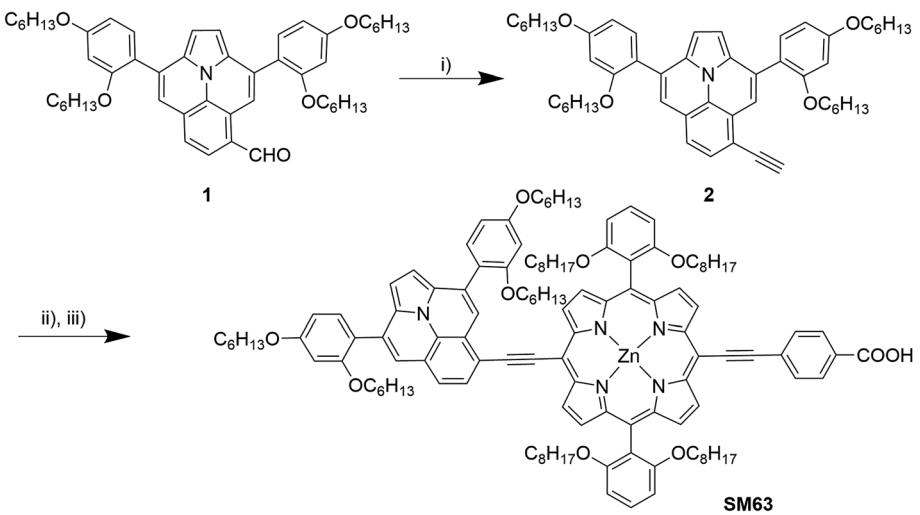

Scheme 1 Synthesis of the SM63 sensitizer. Conditions (i) $(CHBr_2)Ph_3PBr$, *t*-BuOK, THF, −78 °C, 1.5 h, 71%. (ii) **3**, $Pd(PPh_3)_4$, CuI, THF, Et_3N, (iii) 4-ethynylbenzoic acid, $Pd(PPh_3)_4$, CuI, THF, Et_3N, 3 h, 26% (over 2 steps).

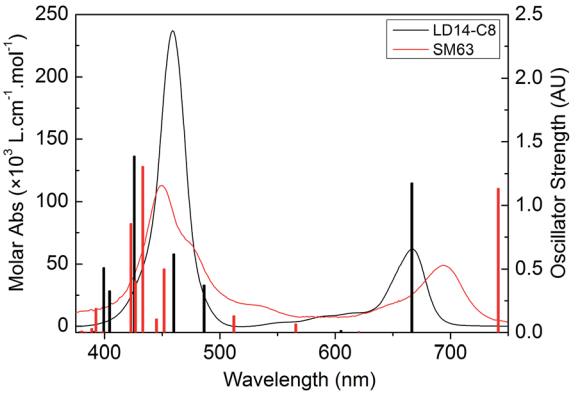

Fig. 2 Absorption spectra of the SM63 (red) and LD14-C8 (black) dyes. The experimental spectra (in THF) are shown as continuous lines and the theoretical electronic transitions are shown as bars. Theoretical data were computed using LR-TDDFT/M06/IEFPCM(THF).

at 474 nm, however the calculated excitations for this dye reveal that the broadening of the Soret band is due a contribution of several new excitations. This is in stark contrast to the absorption spectrum of **LD14-C8** possessing a singular Soret absorption peak at 459 nm that exhibits twofold molar absorptivity, originating from the greater degree of electronic symmetry within **LD14-C8**, evident in both experimental and calculated absorption spectra. Introduction of ullazine as a donor motif in **SM63** resulted in a drastic deformation of the B-band of the porphyrin, as a result of the increase in conjugation along the donor–acceptor axis of the dye, which allows differentiation between the two electronic transitions that give rise to the Soret band (in an electronically symmetrical porphyrin).[4,20–22] Interestingly, the molar absorptivity of the Soret bands experienced a significant decrease in magnitude, implying a decrease in the dipole strength of the transitions leading to these absorptions. However, this splitting of the Soret band in **SM63** into two differentiable peaks improved light harvesting ability of the dye when incorporated into a DSC (*vide infra*). A clear absorption at 530 nm was evident in the UV-Vis spectrum of **SM63**, affording further improvements in light harvesting in the DSC. The lowest energy Q-band absorbance of **SM63** appeared at 693 nm, experiencing a large red-shift compared to **LD14-C8** (667 nm), further reinforcing the advantage of the ullazine donor in enhancing light absorption. In a similar fashion to the Soret absorption in **SM63**, the lowest energy Q-band also experienced a slight decrease in molar absorptivity. The net result of employing the ullazine moiety in the porphyrin dye structure is significant improvement in visible light absorption compared to **LD14-C8**. Furthermore, the ullazine donor in **SM63** extended the π-system of the dye decreasing the optical bandgap to 1.75 eV from 1.84 eV in **LD14-C8**. Combining the optical bandgap and the oxidation potential (*vide infra*) demonstrates that the dye **SM63** possesses frontier orbitals of energy sufficient for thermodynamically favourable electron injection and dye regeneration in the DSC.

Steady-state fluorescence properties

The steady-state emission spectrum (ESI†) of **SM63** afforded an emission maximum at 724 nm, red-shifted significantly from the 680 nm emission of **LD14-C8** (Table 1). The emission spectrum of **SM63** exhibited mirror-image symmetry with the Q-band absorption however the shape of the emission was quite broad compared to **LD14-C8**, indicative of an enhanced charge transfer character in the excited state upon introduction the ullazine moiety as a donor unit.[4] The Stokes shift exhibited in solution for **SM63** was (618 cm^{-1}, 0.0766 eV) dramatically increased from that of **LD14-C8**, (287 cm^{-1}, 0.0356 eV) implying that the introduction of the ullazine donor results in a greater degree of geometry distortion upon formation of the excited state after light absorption. These results are also consistent with the improvements in charge transfer character observed in the calculated absorption and emission spectra (*vide infra*).

Electrochemical properties

Cyclic voltammetry (CV) and differential pulse voltammetry (DPV) were employed to determine the oxidation potential (E_{ox}) of the dye **SM63** (Fig. 3) with the relevant data presented in Table 1. Measurements were performed in DMF with 0.1 M tetrabutylammonium hexafluorophosphate, using a glassy carbon, Pt plate and Pt wire as the respective working, counter and reference electrodes. The corresponding redox potentials were internally referenced using the ferrocene/ferrocenium (Fc/Fc^+) redox couple and the potentials adjusted to values *vs.*

Table 1 Summary of UV-Vis, fluorescence and electrochemical data for SM63 and LD14-C8 Summary of photovoltaic data acquired under standard conditions (AM 1.5G, 1000 W m^{-2}). Data is an average of three devices ($N = 3$, champion data for SM63 in brackets)

Dye	λ_{max}[a]/nm ($\varepsilon/\times10^3$ L cm^{-1} mol^{-1})	λ_{em}[b]/nm	$E_{0\text{-}0}$[c]/eV	E_{ox}[d]/V	E_{red}[d]/V	E^*_{ox}[f]/V	J_{SC} (mA cm^{-2})	V_{OC} (V)	FF	PCE (%)
SM63	450 (113) 474 (67)	724	1.75	0.79	−0.88[e]	−0.96	14.43 ± 0.27	0.70 ± 0.01	0.73 ± 0.01	7.35 ± 0.13
	530 (17) 693 (49)				−1.16		(15.8)	(0.70)	(0.70)	(7.70)
LD14-C8	459 (237)	680	1.84	0.80	−1.12	−1.04	15.72 ± 0.26	0.73 ± 0.02	0.74 ± 0.01	8.45 ± 0.16
	667 (62)	744			−1.59					

[a] Measured in THF. [b] Measured in THF using $\lambda_{ex} = 660$ nm for **LD14-C8** and 475 nm for **SM63**. [c] Determined by the intersection of normalized absorption and emission spectra. [d] Measured in DMF with Fc/Fc^+ as an internal standard and converted to *vs.* NHE by addition of +0.691 V (as Fc/Fc^+ in DMF/NBu_4PF_6 = +0.45 V *vs.* SCE[18] with SCE = +0.241 V *vs.* NHE[19]). [e] Irreversible reduction process. [f] E^*_{ox} is determined from E_{ox} and $E_{0\text{-}0}$.

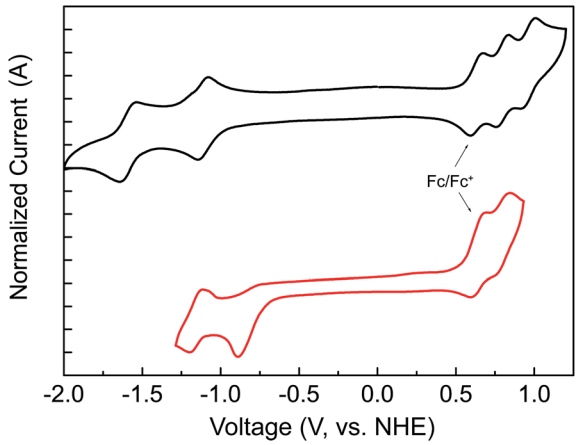

Fig. 3 Cyclic voltammograms of LD14-C8 (black) SM63 (red) and in DMF and ferrocene/ferrocenium internal reference.

NHE by the addition of +0.691 V. The position of E_{ox} is critical in determining the ability of the dye cation, generated after light absorption of the dye in the cell and subsequent electron injection in TiO_2, to successfully undergo regeneration with the I^-/I_3^- redox couple. A quasi-reversible E_{ox} at +0.79 V *vs.* NHE was observed for **SM63.** The dye also experiences two reductions at −0.88 and −1.16 V, the first being irreversible in nature. A decrease in the electrochemical bandgap (1.92 V and 1.67 V for **LD14-C8** and **SM63** respectively) was observed due to the significant increase in π-conjugation within the molecule through incorporation of the ullazine donor. Discrepancy between our data and the previously reported redox data for **LD14-C8** can be rationalized by the use of different solvent for electrochemical analyses (*i.e.* DMF in this work and THF in previous work).[18] The excited state potential (E^*_{ox}) was determined by employing optical and electrochemical data and found to be more negative than the TiO_2 conduction band, allowing sufficient overpotential for thermodynamically favourable electron injection from the dye into the semiconductor's conduction band.

Computational characterisation

The optical and electrochemical characterization of **SM63** and **LD14-C8** were subjected to a complementary investigation by employing DFT/M06/IEFPCM(THF) calculations for geometry optimization and LR-TDDFT/M06/IEFPCM(THF) to determine excitation energies. Complete details of the calculations are given in the ESI.†

The ground state dipole moment of **SM63** was calculated to be 8.07 D, lower than that of the 9.85 D calculated for **LD14-C8.** The frontier Kohn–Sham orbitals of the geometry optimized ground state structures of **SM63** and **LD14-C8** are presented in Fig. 4. In contrast to the planar **LD14-C8,** the calculated structure of **SM63** revealed a deviation of the alkyne-linked ullazine donor and the porphyrin core from planarity, with a bend angle of 20°.

The origin of this donor bending was surmised to be the result of a non-covalent interaction between the two π-systems of **SM63.**

In order to gain further insight this donor-bent geometry was rigorously validated by a series of parallel geometry optimizations that employed different functionals that either largely ignore (BLYP[23–26]) or account (Grimme-D2)[26] for subtle dispersion forces, explained with greater discussion within the ESI.†

This strategy has been used extensively in ascertaining the nature of non-covalent interactions in aromatic systems.[27,28] These parallel calculations revealed that unlike the overwhelming majority of porphyrin-based dyes, which gain stability from maintaining a well-conjugated planar structure, **SM63** sacrifices a small component of electronic conjugation to attain additional stability *via* van der Waals interactions and dispersion forces. This interaction occurs between the bulky

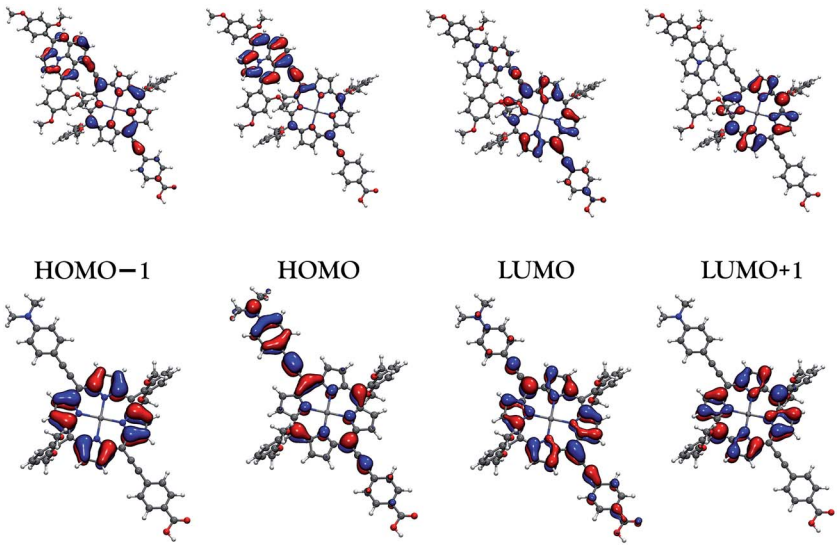

Fig. 4 Contour plots of frontier KS orbitals. The orbitals are calculated for geometry-optimized SM63 (top) and LD14-C8 (bottom), using DFT/M06/IEF-PCM(THF) (isovalue = 0.02 a.u.).

aromatic groups of the ullazine and porphyrin (*meso*-positions) moieties, leading to ground state deformation. The vertical ionization energies (IE) were computed at (U)DFT/M06 level of theory for both dyes calculations showing that the ionization energy of **SM63** (4.67 eV) was slightly lower than that of **LD14-C8** (4.86 eV). However, this trend correlates well with the electrochemically measured E_{ox} for the two compounds (Table 1) and imply a weak destabilisation of **SM63** HOMO as a result of introducing the ullazine core as a donor. Ullazine, being a stronger electron donor (when connected to the porphyrin through the 5-position of the ullazine core[16]) than dimethylaniline, raises the HOMO energy level and reduces the bandgap which in turn induces a greater red shift to its spectrum compared to **LD14-C8**. In contrast to the majority of reported porphyrin dyes which are green in colour, **SM63** appears brown/black as a solid, and affords a brown solution as a result of broader absorption in the range of 500–620 nm. LR/TDDFT results show two transitions of reasonable oscillator strength in this range for **SM63** (512 nm and 566 nm) whereas only one very weak transition at 605 nm is present for **LD14-C8**. The character of the lower energy (566 nm) excitation of **SM63** in this region between the Soret and Q-bands is mostly (78%) composed of HOMO − 1 to LUMO transition, where the HOMO − 1 is highly delocalized on the ullazine moiety (this is also apparent in Fig. 4). The analogous transition for **LD14-C8** (605 nm), is mostly composed of HOMO to LUMO + 1 transition (60%). From this data, we can surmise that the presence of the ullazine leads to a greater delocalization of the highest occupied orbitals in **SM63** compared to those of **LD14-C8**, and increases the charge-transfer character of the corresponding transitions. This is best depicted in the density difference contour plot for the S0 → S1 transition (Fig. 5).

In addition to elucidation of the geometric and electronic ground state properties of **SM63**, we employed a computational method to gain further insight into the structural changes that occur in the excited state, which lead to the significant increase

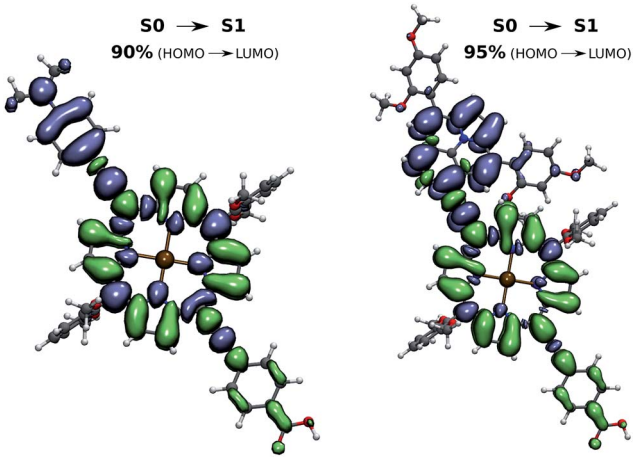

Fig. 5 Contour plots of electron–hole density map of [S0 → S1] vertical transition for **LD14-C8** (left) and **SM63** (right). The density difference contour plots ($\rho_{S1} - \rho_{S0}$) show the electron distribution in green and the hole in blue (isovalue = 0.0003 a.u.).

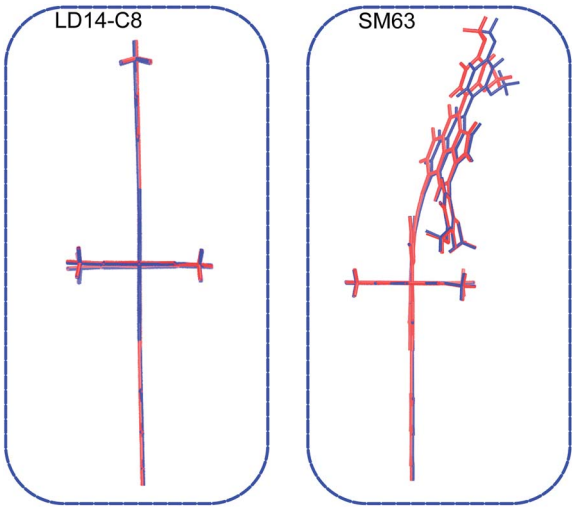

Fig. 6 Side views of **LD14-C8** (left) and **SM63** (right) in their respective ground (red) and first excited (blue) states. Donor-bending in the excited state **SM63** is origin of the considerable Stokes shift observed computationally and experimentally.

(measured spectroscopically) in Stokes shift for **SM63**. Briefly, calculated Stokes shifts were obtained by subtracting the energies of the first absorption and emission transitions of the respective ground state and the first excited state optimized (LR-TDDFT) structures, with a detailed discussion in the ESI.† Thus, calculated Stokes shifts of 0.2377 eV and 0.2071 eV were obtained for **SM63** and **LD14-C8** respectively, consistent with the trend in the spectroscopically derived values. Geometry optimization of the first excited state was performed to computationally assess the degree of conformational distortion that the dye sustains upon excitation from the ground state, with the result given in Fig. 6. Indeed, the excited state geometry of **SM63** demonstrated a greater deviation than **LD14-C8** from its ground state geometry. Specifically, the **SM63** dye distorts at the acetylenic bridge between ullazine and porphyrin systems, with the bend angle of the alkyne changing from 20° to 24° in the excited state, thus underpinning the point of molecular reorganization responsible for the considerable Stokes shift observed spectroscopically. In contrast, the excited state of **LD14-C8** experiences a negligible degree of distortion from its ground state geometry, consistent with the small Stokes shift observed both computationally and experimentally.

Photovoltaic properties

SM63 was implemented into DSCs employing a photoanode with a double layer structure, consisting of 10 μm transparent (20 nm TiO_2) and 3 μm scattering layer (400 nm TiO_2) with a total area of 0.25 cm^2. The fabrication procedure is similar to that reported previously.[29] The TiO_2 electrode was immersed in a solution of **SM63** prior to washing with acetonitrile and sealing (Surlyn, 25 μm) with a platinized FTO counter electrode. An electrolyte consisting of 1.0 M 1,3-dimethylimidazolium iodide (DMII), 0.03 M I_2, 0.05 M LiI, 0.1 M GuNCS, 0.5 M 4-*t*-butylpyridine in acetonitrile was introduced by vacuum backfilling prior to sealing with

Surlyn and a glass cover slide. Measurements were performed using a non-reflective metal mask (area 0.16 cm^2) under standard global AM 1.5G illumination (1000 W m^{-2}).

Optimization of DSC fabrication conditions was performed by initially employing a THF/EtOH (1 : 4) solution of **SM63** (0.2 mM) and 1 mol equivalent of CDCA (0.2 mM). Initial optimizations were performed on the dipping time, with the result given in Fig. S2 and summarized in Table S1.† The J_{SC} (10.9 mA cm^{-2}) and PCE (5.25%) peaked after a 30 minute sensitization, with the J_{SC} and FF decreasing with longer dipping times, indicative of excessive aggregation during sensitization. This is not surprising, considering the extensive planar, aromatic surface area and substantial hydrophobicity of the dye **SM63**.

Increasing the CDCA concentration tenfold (2 mM), afforded a significant improvements J_{SC} (12.6 mA cm^{-2}) and V_{OC} (0.71 V) with a slightly longer (1 hour) sensitization time to achieve a PCE of 5.90% (Fig. S2 and Table S1†). To further suppress aggregation of **SM63** in the dipping solution, the polarity of the solvent was decreased by employing toluene in place of THF and decreasing the amount of ethanol in the dipping solution (*i.e.* toluene/EtOH, 1 : 1). This strategy yielded the best result, affording further improvements in J_{SC} and PCE (*vide infra*).

Fig. 7a shows the photocurrent–voltage characteristics of DSCs fabricated with **SM63** and **LD14-C8** as a sensitizer, with the photovoltaic data summarized in Table 1. The current–voltage characteristics of **SM63** demonstrated a short-circuit photocurrent (J_{SC}) of 14.43 mA cm^{-2}, open-circuit voltage (V_{OC}) of 0.70 V, fill factor (FF) of 0.73 and a power conversion efficiency (PCE) of 7.35%. Conversely, **LD14-C8** achieved a J_{SC} of 15.72 mA cm^{-2}, V_{OC} of 0.73 V, FF of 0.74 and a PCE of 8.45%.

The lower observed J_{SC} for DSCs fabricated with **SM63** can be rationalized by the significant degree of aggregation that the dye experiences upon adsorption to the surface, leading to undesirable quenching of the excited state dye. This is evidenced by improvements in the dye adsorption upon the addition of CDCA and the use of a less polar adsorption solvent (*vide supra*). Further to this, **SM63** features a lower extinction coefficient that may result in a lower degree of light harvesting by the cell.

Rationalization of the reduction of V_{OC} experienced by DSCs using **SM63** required further investigation employing transient photocurrent and photovoltage measurements, where a reduction in V_{OC} can arrive by (a) enhanced recombination of injected electrons from TiO_2 to the dye/electrolyte or (b) a downward shift of the TiO_2 conduction band.[30–32]

Measurement of the electron lifetime as a function of chemical capacitance C_μ (Fig. 7b) afforded insight into the recombination events that occur at the TiO_2–dye/electrolyte interface in DSCs fabricated with **LD14-C8** and **SM63** within the TiO_2 film.[33] At a given C_μ, the electron lifetimes of **SM63** and **LD14-C8** are identical and therefore the decrease in V_{OC} in DSCs featuring **SM63** cannot be assigned to an increase in recombination at the TiO_2–dye/electrolyte interface.

Fig. 7c shows the measurement of the chemical capacitance (C_μ) with respect to V_{OC} gives a direct insight into the conduction band level in devices featuring both **SM63** and **LD14-C8**, as C_μ and DOS are proportional to each other. The plot demonstrates that sensitization with **SM63** results in a displacement of

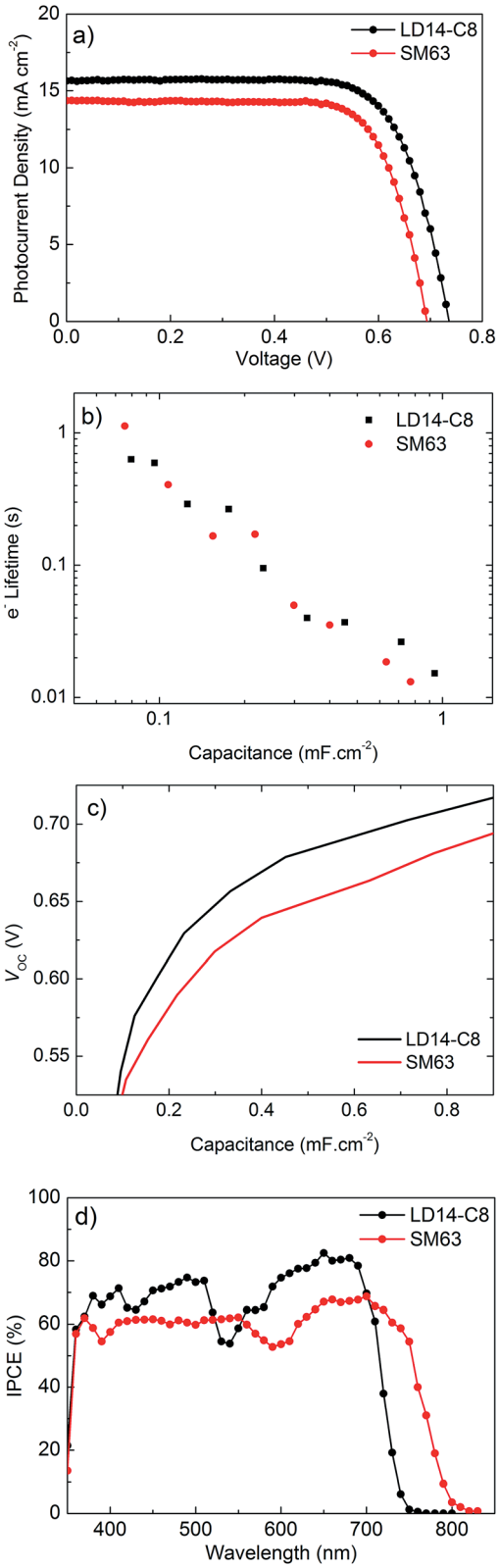

Fig. 7 (a) J–V curve ($N = 3$ cells) of **LD14-C8** (black) and **SM63** (red) under AM 1.5G illumination (1000 W m^{-2}). (b) Electron lifetime and (c) open-circuit voltage as a function of chemical capacitance obtained through transient photocurrent/photovoltage measurements (d) photocurrent action spectrum of **LD14-C8** (black) and **SM63** (red).

trap-state distribution to lower energies, ultimately resulting in a reduction of V_{OC} in the DSC. This is further supported by the previous observation that a reduction in dipole moment (8.07 D and 9.85 D for **SM63** and **LD14-C8** respectively) has been shown to promote a decrease in V_{OC} as a result of a TiO_2 conduction band shift with respect to the redox potential of the electrolyte, which is partially followed by the energy level of the dye.[34]

The photocurrent action spectra of **LD14-C8** and **SM63** are presented in Fig. 7d. **LD14-C8** presents a high IPCE across the visible spectrum with the characteristic dip at ~550 nm (an artefact from the lack of absorbance between Soret and Q-band transitions) and an onset at 750 nm, affording the resulting cell a green colour. In contrast, the IPCE of **SM63** presents a gradual decrease in IPCE dip at ~600 nm in combination with a considerable improvement is red light harvesting ability.

The onset of light harvesting for DSCs employing **SM63** appears at 800 nm resulting in a brown coloured cell. This data in particular demonstrates that a significant gain in light harvesting ability can be obtained through using the ullazine as an electron donor. Presumably, part of the large red shift in the photocurrent action spectrum that gives rise to the long wavelength light harvesting ability of DSCs fabricated with **SM63** originates from favourable J-aggregation of the dye within the cell.[35] In spite of this, a better balance must be struck between this favourable, organized interaction and deactivation of the dye through excessive, non-productive aggregation, extraordinarily prominent for **SM63**, which is potentially caused by the large planar aromatic structure of the dye.

Conclusions

The synthesis of an ullazine–porphyrin dyad was achieved by Sonogashira coupling of an alkyne-functionalized ullazine and zinc porphyrin. The resulting dye, **SM63**, was additionally functionalized with an ethynylbenzoic acid to enable anchoring to TiO_2 and construction of a DSC. **SM63** was characterized thoroughly and the UV-Vis absorption spectrum demonstrated a significant perturbation of both Soret and Q-band absorbances, a consequence of the strong electron donating ability of the ullazine unit. The absorption changes of **SM63** result in an improved absorption of green (~550 nm) and red (>700 nm) light compared to the vast majority of D–π–A porphyrin dyes. Measurement of steady-state emission spectra afforded an unusually large Stokes shift for **SM63**. A thorough computational study of the ground state geometry of **SM63** gave a structure with a bent donor group due to a significant dispersion force interaction between pendant phenyl groups on the ullazine and porphyrin groups in **SM63**. Geometry optimization of the **SM63** excited state revealed an enhancement of this donor bending giving an origin to the larger stokes shift for **SM63**. Computational methods were employed to analyse the distribution of the frontier orbitals and theoretical electronic transitions of **SM63**. Correlation of the new absorption bands in **SM63** to theoretical electronic transitions provided insight into the improved absorption characteristics of the ullazine–porphyrin construct. Finally the dye **SM63** was employed in a DSC using an iodide/triiodide electrolyte, affording a slightly lower PCE (7.35%) than a standard dye **LD14-C8** (8.45%) under identical conditions, as the dye **SM63** experiences significant aggregation in solution as a result of its large hydrophobic aromatic structure. Strikingly, acquisition of the photocurrent absorption spectrum showed a significantly improved green (550 nm) and red (>700 nm) light harvesting ability originating from the improved absorption properties of the **SM63** dye. Future work seeks to develop a strategy to suppress the unfavourable aggregation of the ullazine–porphyrin construct to obtain yet higher efficiencies. Concomitantly, there is value in demonstrating the potential of the strongly donating ullazine core to strongly perturb the absorption in other π-systems, leading to the development of a new range of panchromatic dyes for application in photo(electro)chemical devices.

Acknowledgements

The research leading to these results received funding from Solvay Fluor GmbH, the European Union Seventh Framework Programme (FP7/2007–2013) under grant agreement 'ENERGY-261920, ESCORT' and SSSTC (Sino-Swiss Science and Technology Cooperation), and the European Community's Seventh Framework Programme (FP7/2007–2013) under grant agreement no. 246124 of the SANS project. M. G. thanks the European Research Council (ERC) for supporting part of this work under the advanced research grant (no. 247404) MESOLIGHT. M. K. N. acknowledges the World Class University programme, Photovoltaic Materials, Department of Material Chemistry, Korea University, Chungnam, 339-700, Korea, funded by the Ministry of Education, Science and Technology through the National Research Foundation of Korea (no. R31-2008-000-10035-0).

Notes and references

1 A. Yella, H. W. Lee, H. N. Tsao, C. Yi, A. K. Chandiran, M. K. Nazeeruddin, E. W. G. Diau, C. Y. Yeh, S. M. Zakeeruddin and M. Grätzel, *Science*, 2011, **334**, 629–634.
2 L. Cabau, C. V. Kumar, A. Moncho, J. N. Clifford, N. López and E. Palomares, *Energy Environ. Sci.*, 2015, **8**, 1368–1375.
3 S. Mathew, H. Iijima, Y. Toude, T. Umeyama, Y. Matano, S. Ito, N. V. Tkachenko, H. Lemmetyinen and H. Imahori, *J. Phys. Chem. C*, 2011, **115**, 14415–14424.
4 S. Mathew, A. Yella, P. Gao, R. Humphry-Baker, B. F. E. Curchod, N. Ashari-Astani, I. Tavernelli, U. Rothlisberger, M. K. Nazeeruddin and M. Grätzel, *Nat. Chem.*, 2014, **6**, 242–247.
5 A. Yella, C. L. Mai, S. M. Zakeeruddin, S. N. Chang, C. H. Hsieh, C. Y. Yeh and M. Grätzel, *Angew. Chem., Int. Ed.*, 2014, **126**, 3017–3021.
6 Y. C. Chang, C. L. Wang, T. Y Pan, S. H. Hong, C. M. Lan, H. H. Kuo, C. F. Lo, H. Y. Hsu, C. Y. Lin and E. W. G. Diau, *Chem. Commun.*, 2011, **47**, 8910–8912.
7 C. L. Wang, C. M. Lan, S. H. Hong, Y. F. Wang, T. Y. Pan, C. W. Chang, H. H. Kuo, M. Y. Kuo, E. W. G. Diau and C. Y. Lin, *Energy Environ. Sci.*, 2012, **5**, 6933–6940.

8 C. H. Wu, T. Y. Pan, S. H. Hong, C. L. Wang, H. H. Kuo, Y. Y. Chu, E. W. G. Diau and C. Y. Lin, *Chem. Commun.*, 2012, **48**, 4329–4331.
9 C. L. Wang, Y. C. Chang, C. M. Lan, C. F. Lo, E. W. G. Diau and C. Y. Lin, *Energy Environ. Sci.*, 2011, **4**, 1788–1795.
10 C. L. Wang, J. Y. Hu, C. H. Wu, H. H. Kuo, Y. C. Chang, Z. J. Lan, H. P. Wu, E. W. G. Diau and C. Y. Lin, *Energy Environ. Sci.*, 2014, **7**, 1392–1396.
11 J. Luo, M. Xu, R. Li, K. W. Huang, C. Jiang, Q. Qi, W. Zeng, J. Zhang, C. Chi, P. Wang and J. Wu, *J. Am. Chem. Soc.*, 2014, **136**, 265–272.
12 Y. Xie, Y. Tang, W. Wu, Y. Wang, J. Liu, X. Li, H. Tian and W. H. Zhu, *J. Am. Chem. Soc.*, 2015, **137**, 14055–14058.
13 X. Sun, Y. Wang, X. Li, H. Ågren, W. Zhu, H. Tian and Y. Xie, *Chem. Commun.*, 2014, **50**, 15609–15612.
14 H. Balli and M. Zeller, *Helv. Chim. Acta*, 1983, **66**, 2135–2139.
15 F. Gerson and A. Metzger, *Helv. Chim. Acta*, 1983, **66**, 2031–2043.
16 J. H. Delcamp, A. Yella, T. W. Holcombe, M. K. Nazeeruddin and M. Grätzel, *Angew. Chem., Int. Ed.*, 2013, **52**, 376–380.
17 A. Dualeh, R. Humphry-Baker, J. H. Delcamp, M. K. Nazeeruddin and M. Grätzel, *Adv. Energy Mater.*, 2013, **3**, 496–504.
18 N. G. Connelly and W. E. Geiger, *Chem. Rev.*, 1996, **96**, 877–910.
19 A. J. Bard and L. R. Faulkner, *Electrochemical Methods: Fundamentals and Applications*, Wiley, New York, 2001.
20 M. Kasha, H. R. Rawls and M. A. El-Bayoumi, *Pure Appl. Chem.*, 1965, **11**, 371–392.
21 M. Gouterman, *J. Chem. Phys.*, 1959, **30**, 1139–1161.
22 M. Gouterman, *J. Mol. Spectrosc.*, 1961, **6**, 138–163.
23 A. D. Becke, *Phys. Rev. A*, 1988, **38**, 3098–3100.
24 Y. Zhao and D. G. Truhlar, *J. Chem. Theory Comput.*, 2005, **1**, 415–432.
25 Y. Zhao and D. G. Truhlar, *J. Chem. Theory Comput.*, 2007, **3**, 289–300.
26 S. Grimme, *J. Comput. Chem.*, 2006, **27**, 1787–1799.
27 D. Řeha, M. Kabeláč, F. Ryjáček, J. Šponer, J. E. Šponer, M. Elstner, S. Suhai and P. Hobza, *J. Am. Chem. Soc.*, 2002, **124**, 3366–3376.
28 S. E. Wheeler, *Acc. Chem. Res.*, 2013, **46**, 1029–1038.
29 S. Ito, T. N. Murakami, P. Comte, P. Liska, C. Gratzel, M. K. Nazeeruddin and M. Gratzel, *Thin Solid Films*, 2008, **516**, 4613–4619.
30 P. R. F. Barnes, K. Miettunen, X. Li, A. Y. Anderson, T. Bessho, M. Grätzel and B. C. O'Regan, *Adv. Mater.*, 2013, **25**, 1881–1922.
31 B. C. O'Regan and F. Lenzmann, *J. Phys. Chem. B*, 2004, **108**, 4342–4350.
32 B. C. O'Regan, K. Bakker, J. Kroeze, H. Smit, P. Sommeling and J. R. Durrant, *J. Phys. Chem. B*, 2006, **110**, 17155–17160.
33 K. B. Aribia, T. Moehl, S. M. Zakeeruddin and M. Grätzel, *Chem. Sci.*, 2013, **4**, 454–459.
34 S. Rühle, M. Greenshtein, S. G. Chen, A. Merson, H. Pizem, C. S. Sukenik, D. Cahen and A. Zaban, *J. Phys. Chem. B*, 2005, **109**, 18907–18913.
35 S. L. Li, K. J. Jiang, K. F. Shao and L. M. Yang, *Chem. Commun.*, 2006, **42**, 2792–2794.